Charge transfer doping of graphene without degrading carrier mobility

Cite as: J. Appl. Phys. **121**, 224304 (2017); https://doi.org/10.1063/1.4985121
Submitted: 28 April 2017 . Accepted: 25 May 2017 . Published Online: 13 June 2017

Haichang Lu, Yuzheng Guo, and John Robertson

Charge transfer doping of graphene without degrading carrier mobility

Haichang Lu,[1] Yuzheng Guo,[2] and John Robertson[1,a)]
[1]*Department of Engineering, Cambridge University, Cambridge CB2 1PZ, United Kingdom*
[2]*College of Engineering, Swansea University, Swansea SA1 8EN, United Kingdom*

(Received 28 April 2017; accepted 25 May 2017; published online 13 June 2017)

Density functional calculations are used to analyze the charge transfer doping mechanism by molecules absorbed onto graphene. Typical dopants studied are $AuCl_3$, $FeCl_3$, SbF_5, HNO_3, MoO_3, Cs_2O, O_2, and OH. The Fermi level shifts are correlated with the electron affinity or ionization potential of the dopants. We pay particular attention to whether the dopants form direct chemisorptive bonds which cause the underlying carbon atoms to pucker to form sp^3 sites as these interrupt the π bonding of the basal plane, and cause carrier scattering and thus degrade the carrier mobility. Most species even those with high or low electronegativity do not cause puckering. In contrast, reactive radicals like -OH cause puckering of the basal plane, creating sp^3 sites which degrade mobility. *Published by AIP Publishing.* [http://dx.doi.org/10.1063/1.4985121]

I. INTRODUCTION

Graphene is a two-dimensional material with a unique band structure with bands crossing at the Dirac point.[1] This gives graphene a very high carrier mobility, but the carrier concentration is small, so that its overall electrical conductivity is rather low.[2] Thus, graphene must be doped to increase its carrier concentration and conductivity in order to realize some of its applications such as a transparent electrode in displays or photovoltaic devices[2–6] or as a sensor.[7–9] However, the doping should not degrade its mobility by for example, introducing Coulombic scattering centers. These would reduce the mobility μ according to $\mu = a/N$ dependence,[10] where N is the number of centers. This could lead to no net increase in conductivity in an extreme case. Nor should doping interfere with the uniform π bonding of the graphene sheet by converting sp^2 sites to sp^3.

The conventional way to dope a 3-dimensionally bonded semiconductor would be by substitutional doping. This has indeed been carried out for graphene using nitrogen or boron doping.[11–13] Substitutional sites are advantageous in being fully bonded into the lattice and are thus stable. However, nitrogen can enter the graphene lattice in various configurations, only one of which is an actual doping configuration.[13,14] The other configurations not only do not dope, they also introduce defects[15,16] which cause carrier scattering. This "functionalization" is useful in other contexts such as creating catalytic sites on carbon nanotubes.[15] On the other hand, for graphene as an electrode, it is useful to consider interstitial or charge transfer doping by physisorbed species.[17–24] These can dope the graphene n-or p-type, without necessarily creating defects. Transfer doping is also useful to increase the conductivity of contacts, as the high resistance of contacts to graphene in devices can limit the device performance. The transfer doping method is also relevant to doping of other 2D systems like MoS_2 and is frequently used in organic electronics.

However, a critical factor not previously studied is whether the dopant forms a weak physisorptive bond or strong chemisorptive bond to the graphene. For the first case, this will allow charge transfer (Fig. 1), without modifying the π bonding of the graphene layer and so it should maintain the mobility of the graphene. On the other hand, if a short chemisorptive bond is formed, this will convert the underlying C sp^2 site to sp^3, so removing the π orbital of that site and degrading the graphene mobility.

Here, we study the charge transfer doping caused by a range of dopants. Some of these were previously used in the intercalation of graphite,[25,26] or the charge transfer doping of organic molecules such as in organic light emitting diodes.[27,28] It turns out that some of the dopants have very large electronegativities compared to elemental metals, or are strongly electropositive. Interestingly, we find that even strongly electronegative or electropositive species need not form chemisorptive bonds and so are good transfer dopants.

II. METHODS

The calculations are carried out using periodic supercell models of graphene and the dopant species using the CASTEP plane-wave density functional theory (DFT) code,[29] with ultra-soft pseudopotentials and the Perdew-Burke-Ernzerhof (PBE) form of the generalized gradient approximation (GGA) for the electronic exchange-correlation functional. For an open shell magnetic system like $FeCl_3$, we use the GGA + U method, with an on-site potential U of 7 eV applied to the Fe 3d states. The screened exchange hybrid functional[30] is also used to correct the GGA band gap error in the Cs_2O system.

The dispersion correction to the GGA treatment of the van der Waals interaction is included using the Tkatchenko-Scheffler (TS) version[31] of the Grimme[32] scheme. To overcome the error induced by periodical mirror charge, self-consistent dipole correction is implemented. The plane-wave cut-off energy is 380 eV, as the cut-off energy of oxygen.

For the graphene plus dopant system, a layer-by-layer stacked supercell is created in each case, with a close degree

a)Author to whom correspondence should be addressed: jr@eng.cam.ac.uk

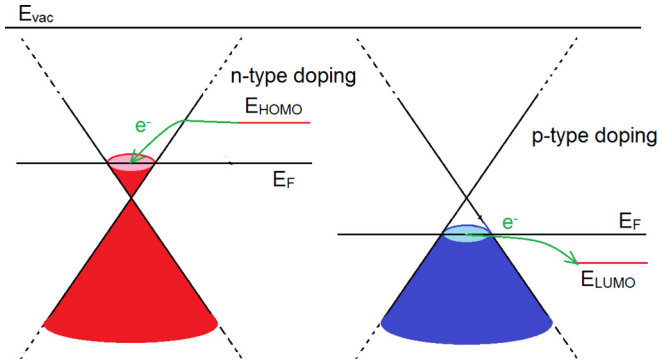

FIG. 1. Schematic of the n-type and p-type doping process in graphene.

of lattice matching between the graphene and the dopant. A 30 Å vacuum layer is included where a vacuum layer is needed. The matching of the graphene and dopant lattices is given in Table I. A dense 9×9 k-point mesh is used to calculate the density of states (DOS), due to the small density of states of graphene close to the Dirac point. The calculated lattice constant of graphene in PBE is 2.47 Å, 0.4% less than the experimental value.[1] The physisorptive binding energy, relevant bond lengths, and any puckering of the graphene sites below the dopant site are given in Table II.

Doping causes a shift in the system's Fermi energy away from the Dirac point of the graphene,[33] as in Fig. 1. This shift is compared to the Fermi energy, ionization potential (IP), or electron affinity (EA) of the isolated dopant system. These energies are calculated using a periodic supercell of the dopant species plus vacuum gap. The electrostatic potential is calculated for the dopant system layers, averaged along the layers. The potential in the vacuum gap region gives the vacuum potential. The energy of the valence band maximum is then compared to the vacuum energy to give the ionization potential, and with the band gap, the electron affinity.

III. RESULTS

We first consider Lewis acids such as $AuCl_3$ and $FeCl_3$. $FeCl_3$ has been more heavily studied, but $AuCl_3$ is simpler computationally because it does not contain d electrons. Crystalline $AuCl_3$ consists of stacked layers of Au_2Cl_6 molecular units. The Au_2Cl_6 molecule consists of two planar edge-connected $AuCl_4$ squares. The supercell consists of

TABLE I. Supercell and lattice match of graphene and dopant. M in the mismatch column refers to a molecular dopant where there is no mismatch.

	Graphene supercell/dopant supercell	Mismatch ratio (%)
SbF_5	$\sqrt{3} \times \sqrt{3}/1 \times 1$	1.66
$FeCl_3$	$\sqrt{7} \times \sqrt{7}/1 \times 1$	1.42
$AuCl_3$	$4 \times 4/1 \times 1$	M
MoO_3	$3 \times \sqrt{3}/2 \times 1$	0.34, 7.92
Cs_2O	$\sqrt{3} \times \sqrt{3}/1 \times 1$	1.62
Cl_2	5×5	M
O_2	5×5	M
OH	5×5	M
HNO_3	5×5	M

TABLE II. Atomic distance, bond length, and puckering of graphene.

	Bond type	Bond (Å)	Surface distance (Å)	Puckering (Å)
OH	O-H	0.98	…	0.51
	C-O	1.51	…	
O_2	O-O(in O_2)	1.24	3.29	0.09
HNO_3	O-H(in H_2O)	0.98	3.28	0.06
	N-O(in NO_2)	1.23	2.60	
	N-O(in NO_3)	1.27	3.25	

alternate graphene and $AuCl_3$ layers along the z axis. Figure 2(a) shows the 4×4 graphene supercell with the planar Au_2Cl_6 units separated from each other in-plane at a similar distance as in pure $AuCl_3$. The position of Au_2Cl_6 units on the graphene layer is allowed to vary to minimize the total energy.

Figure 2(c) shows the band structure of isolated pure Au_2Cl_6 in the hexagonal lattice. Au_2Cl_6 is a semiconductor with a band gap of 1.22 eV. The Au 5d band is filled to $d^{9.6}$. The conduction band consists of the Au s state and Cl p states. Figure 2(d) shows the band structure of the combined system. As a 4×4 supercell was used, the graphene Dirac point still lies at K, and can be recognized as the crossed bands at 1.02 eV. This shows that the shift of the Fermi energy E_F due to this $AuCl_3$ doping concentration is 1.02 eV.

Figure 2(b) shows these results in a density of states (DOS) plot. The doping has occurred by a transfer of electrons from the graphene valence band to the $AuCl_3$ conduction band, filling its conduction bands lying just below 0 eV in the central panel of Fig. 2(b). (If any Cl vacancies form, they are shallow donors, and these would also become filled by the transfer doping.) The carbons of the graphene lattice are found to maintain their planar geometry and do not buckle. The dopant-C separation is 3.35 Å (Table III), so the bond is weak and physisorptive, and no puckering of the underlying C site occurs. This will cause no reduction in mobility.[34]

We next consider $FeCl_3$, which is also a Lewis acid like $AuCl_3$. It has been used extensively as an intercalant of graphite,[35–41] as discussed by Li and Yue.[41] Solid $FeCl_3$ forms a layered system of Fe_2Cl_6 edge-connected octahedra connected along three directions at 120° to each other. The Cl sites are rotated slightly off the vertical. A hexagonal supercell lattice of graphene and $FeCl_3$ can be made with a large 23 Å periodicity.[35] On the other hand, we created a smaller, more efficient $\sqrt{7} \times \sqrt{7}$ supercell using a 1×1 periodicity of the $FeCl_3$ sublattice and a $\sqrt{7} \times \sqrt{7}$ periodicity of the graphene, as in Fig. 3(a). $FeCl_3$ is a magnetic semiconductor with a 0.7 eV band gap. A vertical stacking of one $FeCl_3$ layer and one graphene layer along Oz is ferromagnetic. A stacking of two $FeCl_3$ layers and two graphene layers along Oz, as here, allows the $FeCl_3$ to be antiferromagnetically (AF) ordered, which simplifies the band structure plots (the spin-up and spin-down bands are degenerate). Figure 3(c) shows the AF bands of isolated $FeCl_3$ calculated for a value of $U = 7$ eV, with the 0.7 eV band gap. The Fe 3d occupancy is $d^{5.6}$.

Figure 3(d) shows the band structure of the combined system. The graphene Dirac point can be recognized at the K

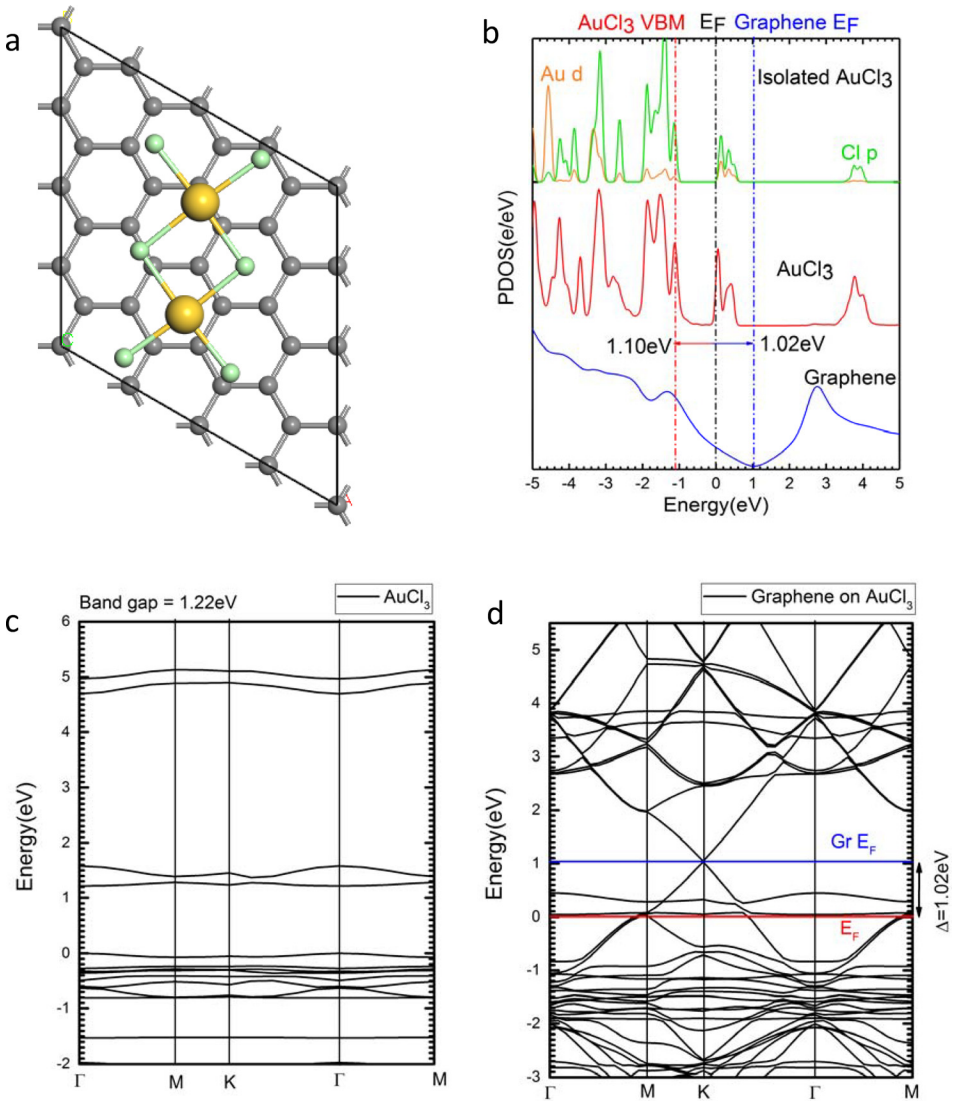

FIG. 2. (a) Au_2Cl_6 molecule on the 4×4 graphene supercell. (b) partial density of states (PDOS) of isolated $AuCl_3$ and $AuCl_3$/graphene system. (c) Band Structure of isolated pure Au_2Cl_6 in the hexagonal lattice. (d) Band Structure of the combined system.

point 1.0 eV above the Fermi energy. Figure 3(b) shows the density of states for the combined system and for the isolated $FeCl_3$. Doping has occurred by transfer of electrons from the upper graphene valence band to the $FeCl_3$ conduction states at −0.1 eV in Fig. 3(b).

As for $AuCl_3$, $FeCl_3$ forms a long physisorptive bond of 3.54 Å to the graphene. No puckering of the underlying carbon site occurs, so the transfer doping of graphene by $FeCl_3$ does not degrade its mobility.

We next consider the strongest Lewis acid, SbF_5. Condensed SbF_5 can be considered to form a network of corner-sharing octahedral with the F sites vertically above each other. The SbF_5 units form chains which are conveniently lattice-matched to graphene, when a supercell of 1×1 SbF_5 and $\sqrt{3} \times \sqrt{3}$ of graphene is used, as in Fig. 4(a).

TABLE III. Calculated layer distance, electron affinity, ionization potential, and Fermi level shift (FLS) from GGA.

	Layer distance (Å)	Electron affinity (eV)	Ionisation potential (eV)	Fermi level shift (eV)
SbF_5	3.65	7.04	10.10	−1.05
$FeCl_3$	3.54	6.42	7.12	−0.92
MoO_3	2.95	6.61	8.64	−0.63
$AuCl_3$	3.35	5.94	7.16	−1.02
Cs_2O	3.75	0.9	2.35	0.95

Figure 4(c) shows the band structure of isolated SbF_5 in the unit cell of Fig. 4(a). It is a semiconductor with a GGA band gap of 3.06 eV, and a direct gap at Γ. This system contains only s, p electrons, and Sb is in its +5 valence state. The top of the valence band consists of F 2pπ states the conduction band minimum consists of empty Sb 5s states. The high electronegativity of F accounts for the large ionization potential of SbF_5 of 11 eV (Table III).

Figure 3(c) shows the band structure of the combined system Due to the orientation of the graphene and SbF_5 sublattices, the Dirac point folds over to appear at Γ, at about 1.0 eV above the combined Fermi energy. Figure 4(d) shows the density of states of the combined system, and of the isolated dopant. Doping has occurred by transfer of electrons from the graphene valence band into the SbF_5 conduction band. This causes a 3.0 eV shift of the SbF_5 bands, but only a 1.2 eV downward shift of E_F in the graphene.

Table III gives the calculated electron affinity, band gap, and ionization potential of these compounds. As ideal isolated semiconductors, their Fermi energies would appear

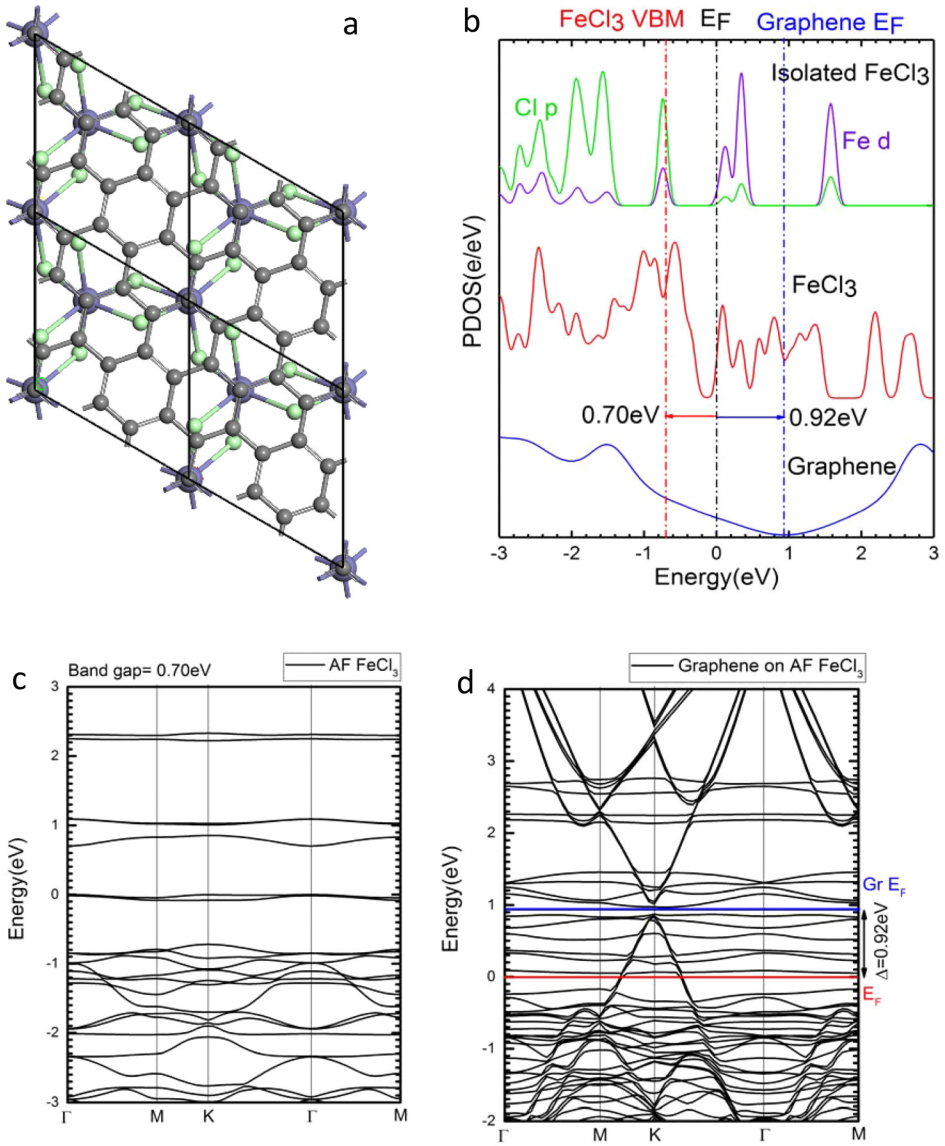

FIG. 3. $FeCl_3$ on the $\sqrt{7} \times \sqrt{7}$ graphene supercell. (b) PDOS of isolated AF $FeCl_3$ and $FeCl_3$/graphene system. (c) Band Structure of isolated pure AF $FeCl_3$. (d) Band Structure of the combined system.

near midgap. In practice, the anion vacancy is the lowest energy defect in these systems, and this defect is calculated to be shallow. Thus, in practice their Fermi energy is likely to lie close to their conduction band edges. The large electronegativity of the halogens means that the valence bands of these systems are very deep below the vacuum level. Even with E_F lying at their conduction band edges, their work functions are still very large, much larger than that of the most electropositive metal, Pt.

We now move to the case of MoO_3. This oxide has been widely used as a p-type dopant and electrode material in organic electronics,[27,28] and has recently been used for p-type doping in carbon nanotubes, graphene,[21,22] and MoS_2 contacts.[42,43] MoO_3 has two forms, the molecule Mo_3O_9, and a layered solid form MoO_3. MoO_3 was previously calculated to have a band gap of 3.0 eV and an electron affinity of 6.6 eV.[44] Its oxygen vacancies were calculated to be shallow. The doping of MoS_2 and carbon nanotubes by MoO_3 layers has already been studied theoretically.[21,43]

An orthorhombic supercell of graphene and MoO_3 was constructed as in Fig. 5(a). The electronic structure of the combined system was calculated. The large work function of MoO_3, 2 eV below that of graphene, means that there is a strong transfer doping. It is found that the Fermi energy of the combined system has shifted downwards in the graphene by 0.63 eV. In this case, doping has occurred by the transfer of electrons from the graphene valence band to the MoO_3 conduction band states. Nevertheless, the bonds between graphene and the outer O layer of MoO_3 are only physisorptive with a bond length of 2.5 Å. MoO_3 does not cause any puckering of the graphene sp^2 sites and thus does not affect the π bonding of the graphene layer. Thus, the C atoms do not act as defects under this doping process. There will be no Raman D peak, and no carrier scattering. This is consistent with experiment where notably Chen *et al.*[17] find that MoO_3 doped graphene retains the ability to show a quantum Hall effect, indicating a high carrier mobility.

MoO_3 is a very valuable dopant of graphene because it is a stable dopant, it raises the carrier concentration, it does not degrade the carrier mobility by causing defects, it has a wide band gap so that it is also optically transparent, a very useful combination useful for optical devices.[18]

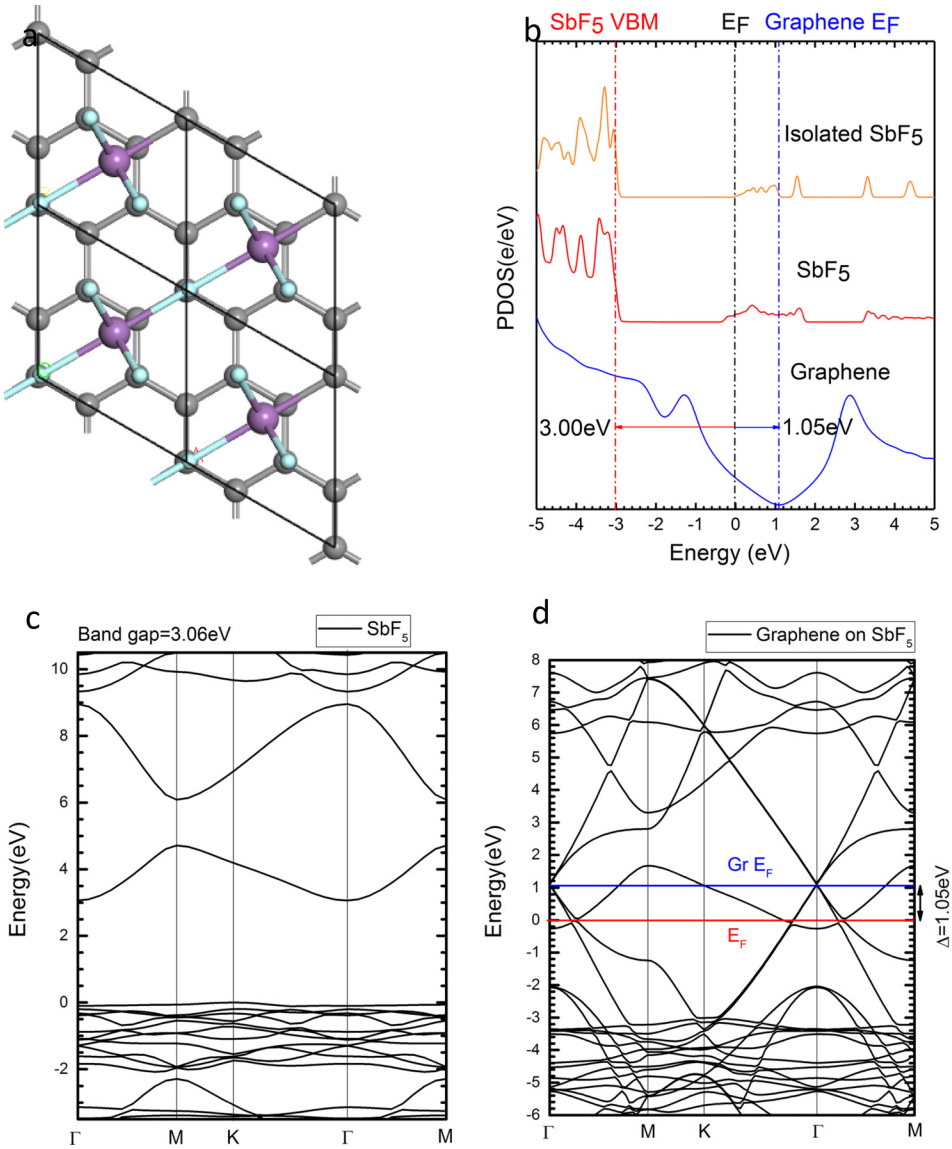

FIG. 4. SbF_5 on the $\sqrt{3} \times \sqrt{3}$ graphene supercell. (b) PDOS of isolated SbF_5 and SbF_5/graphene system. (c) Band Structure of an isolated pure SbF_5 single layer in the hexagonal lattice. (d) Band Structure of the combined system.

We now consider an n-type transfer dopant, CsO_x. Cs carbonate is widely used as an n-type dopant in organic light emitting diodes, and also can be used to dope graphene.[19] The carbonate precursor dissociates on heating to leave a Cs oxide, which may actually be a sub-oxide. We consider the oxide to be Cs_2O. This has the inverse $CdCl_2$ hexagonal layered structure, with the Cs layers on the outside and O atoms on the inside. Note that whereas the interlayer bonding in $CdCl_2$ is van der Waals, the Cs-Cs bonding in Cs_2O is essentially metallic, not van der Waals. The hexagonal layers are reasonably lattice-matched to those of graphene, with a 1.6% mismatch, as shown in Table I and Fig. 6(a). The Cs and O sites lie over the hollow sites of the graphene lattice.

Figure 6(b) shows the band structure of isolated Cs_2O. Cs_2O is a semiconductor with a band gap of 1.4 eV in screened exchange[30] and a very low electron affinity. Its valence band consists of oxygen 2p states. The valence band is very narrow because the O sites are far apart, so the O-O interaction controlling the VB width is weak.

Figure 6(c) shows the density of states for the combined system. There is strong n-type doping, with electrons transferred from the Cs_2O valence band into the graphene conduction band. The E_F of graphene is shifted upwards by 0.95 eV by the Cs_2O layer. Nevertheless, the Cs-C bond is long and physisorptive. It is not van der Waals, and no van der Waals correction to GGA is used in this case. The graphene atoms remain unpuckered below the Cs_2O and the sp^2 bonding is maintained in the graphene. This behavior is similar to the behavior of Cs_2O as an n-type transfer dopant in organic semiconductors.[18]

Nitric acid is another p-type dopant, but it functions differently. Nistor *et al.*[45] studied the absorption of HNO_3 on the graphene surface. They found that HNO_3 could dissociate into an NO_3 radical, a NO_2 radical, and a water molecule

$$2HNO_3 \rightarrow H_2O + NO_2 + NO_3.$$

HNO_3 is introduced into the 5×5 supercell. Dissociation occurs. These species are allowed to rotate to maximize their stability. The final geometry is shown in Fig. 7(a). The NO_3 radical lies planar parallel to the graphene plane, with each

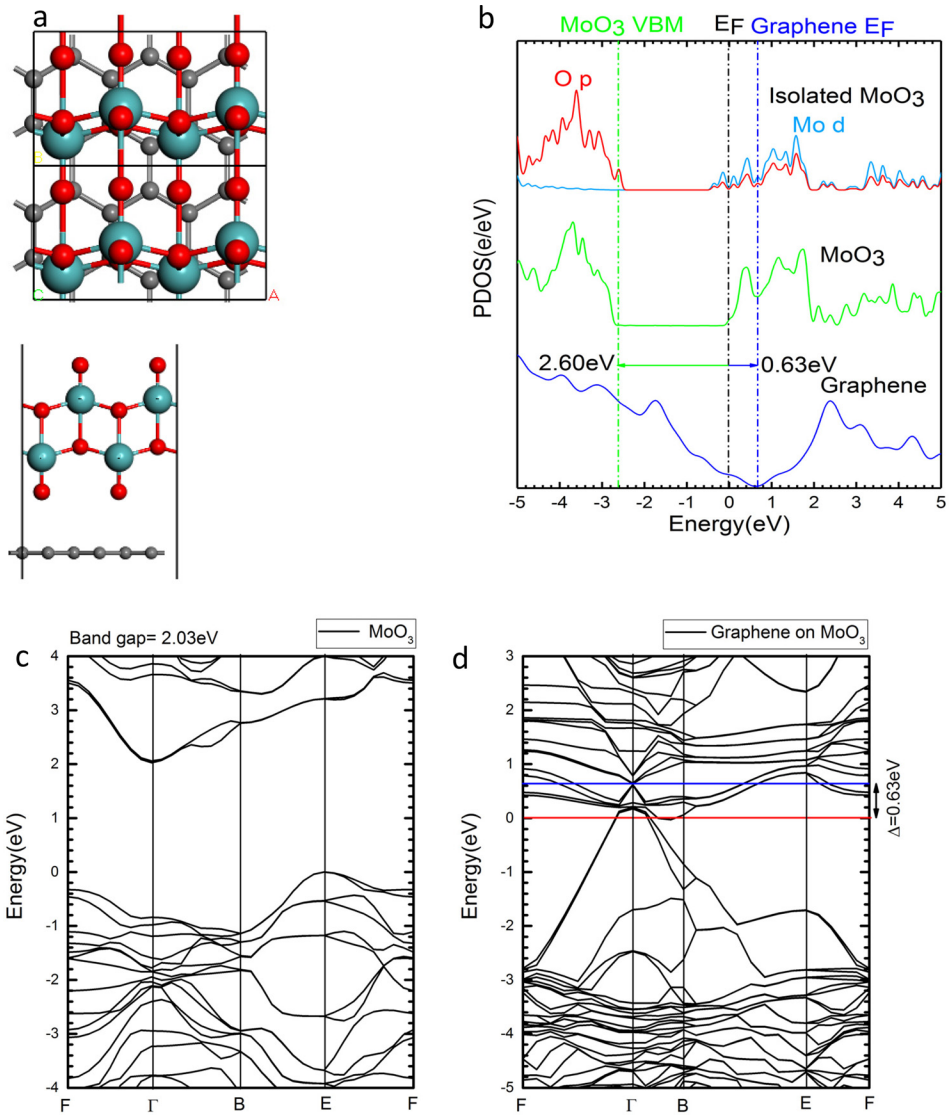

FIG. 5. MoO_3 on $3 \times \sqrt{3}$ graphene supercell. (b) PDOS of isolated MoO_3 and MoO_3/graphene system. (c) Band Structure of isolated pure single layer MoO_3. (d) Band Structure of the combined system.

of its atoms lying on top of a carbon atom. The NO_2 radical and the water molecule lie in a plane normal to the graphene plane, with the central N atom of NO_2 and central O atom of H_2O nose down towards the graphene, as in Fig. 7(b). These species are physisorbed onto the graphene, and the bond lengths are quite large as expected for physisorption (Table II). The water species causes a very weak buckling of the underlying graphene layer, Table II. The binding energy of each species to the graphene is relatively small.

Whereas H_2O is a closed shell system, both NO_3 and NO_2 are radicals each with a half-filled orbital. Critically, the work function of these orbitals is greater than that of the graphene, the states lie deeper below the vacuum level than the Fermi energy E_F of graphene. Thus, they give a singly occupied state lying below E_F. This leads to an electron transfer from the graphene into the two NO_x species, filling their states, and causing a hole doping of the graphene. As the bond length is long, there is only partial charge transfer. The charge transfer is calculated to be $-0.3e$ on the NO_3 and $-0.25e$ on the NO_2. This lowers the E_F of graphene to -0.81 eV, as shown in Fig. 2. The retention of planar sp^2 bonding in the C sites under the NO_3 and NO_2 physisorbed species means that this does not constitute a defect, there is no Raman D peak and no carrier scattering. This is consistent with experiment. D'Arsie[20] finds no change in the D peak intensity experimentally.

We now consider Cl_2. Cl_2 is a closed shell molecule with a single Cl-Cl bond. It has a filled pσ state at -12 eV, two filled pπ states, and two filled pπ^* states, followed by an empty σ^* state above its E_F. The Cl_2 molecule is physisorbed onto graphene, but it does not produce doping because it has no empty states below E_F of graphene [Fig. 8(b)]. There is no doping because the empty σ^* state is high in energy despite the electronegativity of Cl.

Following Cl_2, we consider the O_2 molecule. This molecule is calculated to physisorb in a configuration across a C-C bond, as in Fig. 9(a). Now, the O_2 molecule is geometrically the same as the Cl_2 molecule, but as its valence is lower, its π^* states would be half-filled in the spin unpolarized condition. This configuration is unstable to symmetry breaking to open up a band gap. This occurs by an antiferromagnetic ordering of the σ^* spins, with the up-spin states lying below E_F and the down-spins lying above the gap. For the combined O_2 on the graphene system, the gap is small

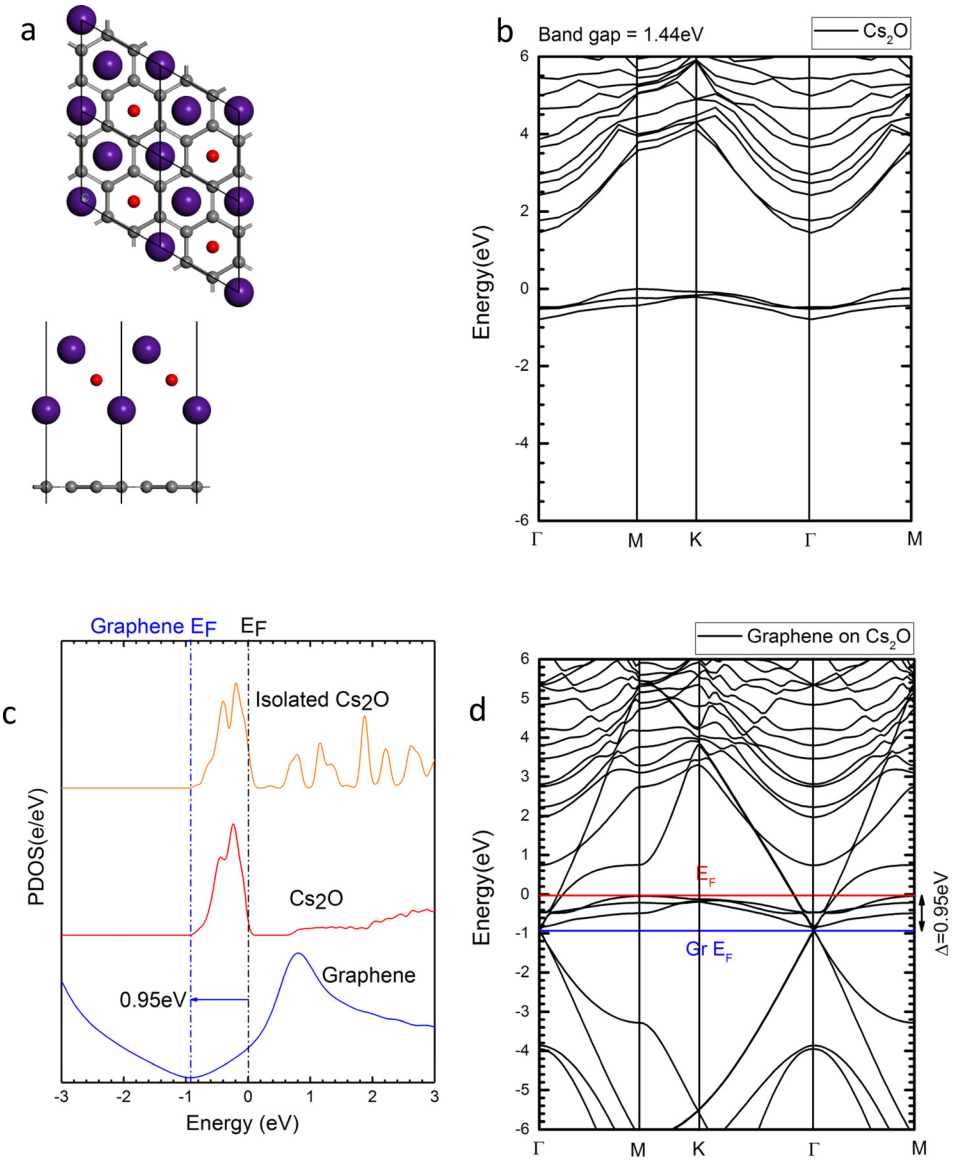

FIG. 6. Top view and side view of Cs_2O on the $\sqrt{3} \times \sqrt{3}$ graphene supercell. (b) Screened exchange band structure of isolated pure single layer Cs_2O. (c) PDOS of isolated Cs_2O and Cs_2O/graphene system. (d) Band Structure of the combined system.

enough that the empty spin-down σ^* state lies below E_F of isolated graphene, so there is a sizable charge transfer doping of the graphene by O_2, as shown in Fig. 9(b). The C-O in this case is long (3.29 Å) and physisorptive.

Finally, we consider the –OH radical. The O-H bond creates a deep-lying filled σ state, and a high-lying empty σ^* state. The other broken O bond makes the unpaired electron of the radical. As O is very electronegative, this p state lies well below E_F of isolated graphene. More interestingly, this p state is able to form a strong C-O bond to a carbon atom underneath, puckering the C atom out of the plane, and converting it into a sp^3 configuration (Fig. 10). Thus, there is charge transfer from the graphene. However, the overall effect on conductivity will be poor because the defect states will lower the mobility.

Overall, except for OH, the various dopants studied here are physisorbed, without puckering the underlying graphene. This occurs because of the strong intra-layer rigidity of graphene, and its resistance to out-of-plane deformation needed to form the fourth extra bond to a chemisorbing species.

IV. COMPARISON TO EXPERIMENT AND DISCUSSION

The electron affinity and ionization potentials of the various dopant species were calculated using dopant supercells as described in Sec. II. The Fermi level shifts (FLS) are compared with the ionization potentials in Table III. The SbF_5, $FeCl_3$, and $AuCl_3$ species have remarkably large ionization potentials, if the band gaps are added to the work functions.

We see that there is monotonic variation of the calculated FLS with the IP. The largest calculated p-type shift occurs for SbF_5, while $FeCl_3$ has the largest shift of the more common dopants $FeCl_3$, $AuCl_3$, and HNO_3. Experimentally, $FeCl_3$ is found to give the largest E_F shift of the common dopants $FeCl_3$, $AuCl_3$, MoO_3, and HNO_3.[36,37]

For MoO_3 doping, our calculations suggest there is no puckering of the underlying C site, so there will be no Raman D peak, and no extra carrier scattering. This is consistent with experiment where notably Chen *et al.*[17] find that MoO_3 doped graphene retains the ability to show a quantum Hall effect, indicating a high carrier mobility.

For $FeCl_3$ doping, our calculations suggest there is no C site puckering, so there will be no Raman D peak and no extra

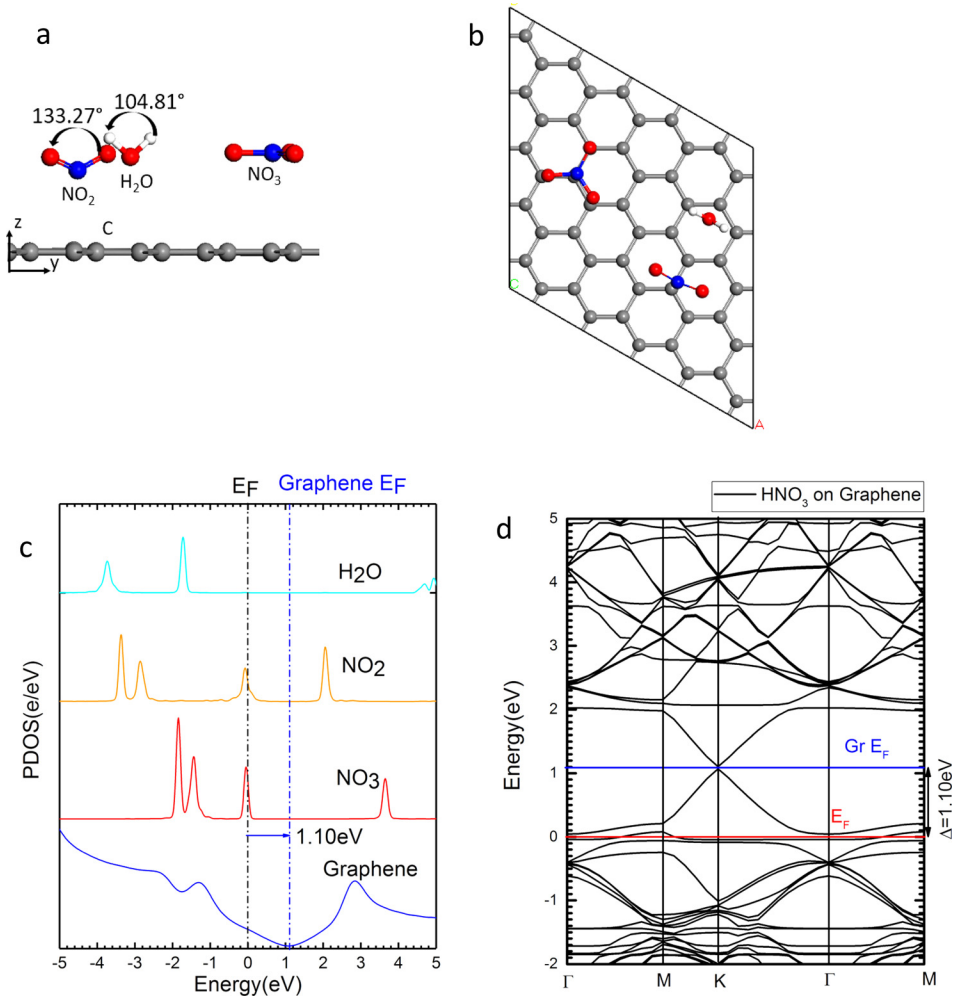

FIG. 7. Side view and (b) top view of $2HNO_3$ dissociated onto a 5×5 graphene supercell. (c) PDOS of $2HNO_3$/graphene system. (d) Band structure of the combined system.

carrier scattering. This is consistent with experiment[26,35–41] although a small D peak does appear in some cases.[39,40]

The absence of a Raman D peak at 1350 cm^{-1} in the experimental works for $FeCl_3$,[26] confirms that $FeCl_3$, MoO_3, and HNO_3 do not give rise to basal plane defects,[17,20,35] and thus should not increase carrier scattering.

Our calculations have a similar aim to those of Hu and Gerber.[33] For $FeCl_3$, our calculations are for the expected spin-polarized state using GGA + U, whereas Liu *et al.*[37] used the spin unpolarized state. We used a more efficient, three times smaller supercell than did Zhan *et al.*[35] by rotating the x, y axes. Overall, the shift of E_F seen in the various calculations of $FeCl_3$ is similar. For HNO_3 doping, we found that the acid dissociates, as in Nistor *et al.*[45] The present paper has considered the widest range of dopant species, including n-type dopants, compared them, and also studied the C site puckering, because it is no use increasing carrier density by doping, if the mobility declines by a similar factor. The main factor that leads to puckering is that the bond to carbon is too strong, for example, from an oxygen radical, and is to be avoided for the most effective form of doping.

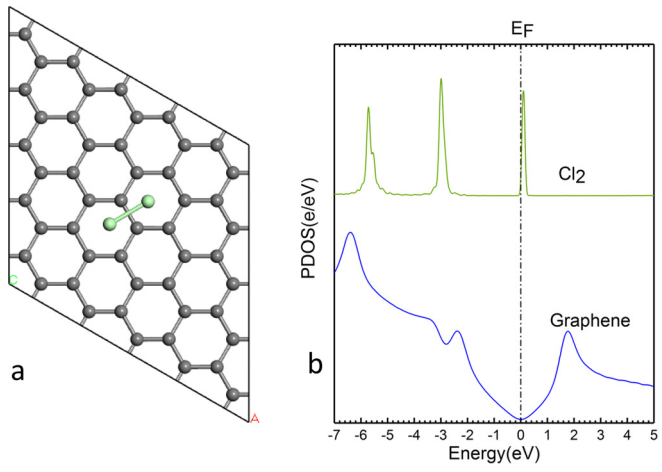

FIG. 8. Top view of Cl_2 on the 5×5 graphene supercell. (b) PDOS of the Cl_2/graphene system.

V. CONCLUSIONS

We have calculated the conditions required for charge transfer doping of graphene (sometimes called non-covalent doping). We find that the Fermi level shift in eV is proportional to the electron affinity of the acceptor species or ionization potential of the donor species. We have treated a wider range of dopant species than other groups. Except for the case of –OH radicals, the dopants physisorb onto the graphene and thus do not create sp^3 "defects" and do not degrade the mobility or cause Raman D peaks. The doping mechanism is similar to that occurring in transfer doping of organic semiconductors.

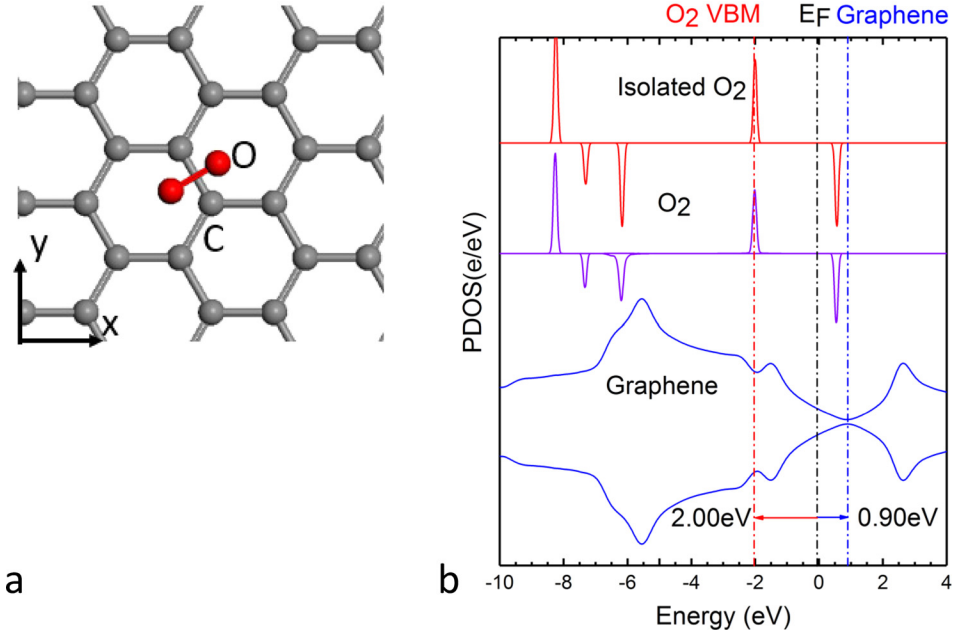

FIG. 9. Top view of triplet O_2 on the 5×5 graphene supercell. (b) PDOS of the O_2/graphene system.

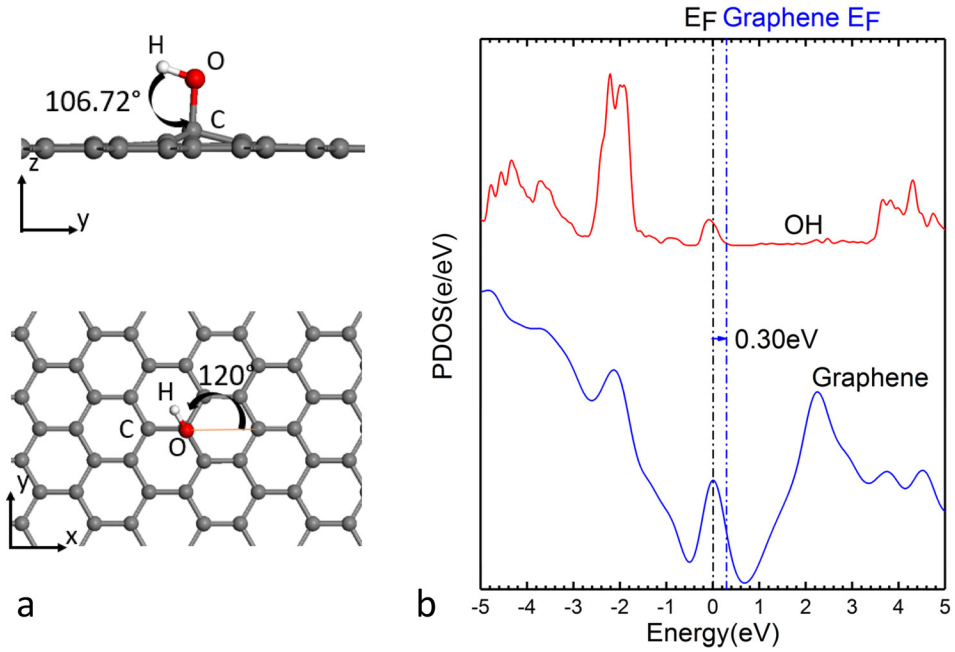

FIG. 10. (a)Side view and top view of OH radical bonding onto 5×5 graphene supercell. (b) PDOS of OH/graphene system.

ACKNOWLEDGMENTS

We thank EPSRC grant EP/P005152/1 and Chinese Scholarship Council for funding.

[1]A. K. Geim and K. S. Novoselov, Nat. Mater. **6**, 183 (2007).
[2]S. De and J. N. Coleman, ACS Nano **4**, 2713 (2010).
[3]S. Bae, H. Kim, and Y. Lee, Nat. Nanotechnol. **5**, 574 (2010).
[4]G. Zhong, X. Wu, L. D'Arsie, and J. Robertson, Appl. Phys. Lett. **109**, 193103 (2016).
[5]S. Sato, Jpn. J. Appl. Phys., Part 1 **54**, 040102 (2015).
[6]S. Hofmann, P. B. Weimer, and R. S. Weatherup, J. Phys. Chem. Lett. **6**, 2714 (2015).
[7]F. Schedin, A. K. Geim, S. V. Morozov, E. W. Hill, P. Blake, M. I. Katsnelson, and K. S. Novoselov, Nat. Mater. **6**, 652 (2007).
[8]T. O. Wehling, K. S. Novoselov, S. V. Morozov, E. E. Vdovin, M. I. Katsnelson, and A. K. Geim, Nano Lett. **8**, 173 (2008).
[9]R. T. Lv, G. G. Chen, Q. Li, A. McCreary, A. Botello-Mendez, S. V. Morozov, L. B. Liang, X. Declerk, N. Perea-Lopez, D. A. Culleni, K. S. Novoselov, and M. Terrones, Proc. Natl. Acad. Sci. U.S.A. **112**, 14527 (2015).
[10]S. Kasap, *Principles of Electronic Materials and Devices* (McGraw-Hill, NY, 2000), p. 351.
[11]Y. C. Lin, C. Y. Lin, and P. W. Chiu, Appl. Phys. Lett. **96**, 133110 (2010).
[12]D. Wei, Y. Liu, Y. Wang, H. Zhang, L. Huang, and G. Yu, Nano Lett. **9**, 1752 (2009).
[13]R. Lv, A. R. Botello-Mendez, T. Hayashi, B. Wang, A. Berkdemir, Q. Hao, A. L. Elias, R. Cruz-Silva, H. R. Gutierrez, Y. A. Kim, H. Muramatsu, H. Terrones, J. V. Charlier, and M. Terrones, Sci. Rep. **2**, 586 (2012).
[14]Y. C. Lin, P. Y. Teng, C. H. Yeh, M. Koshino, P. W. Chiu, and K. Suenaga, Nano Lett. **15**, 7408 (2015).
[15]T. Sharifi, G. Hu, X. Jia, and T. Wagberg, ACS Nano **6**, 8904 (2012).
[16]A. G. Rinzler, J. Liu, H. Dai, P. Nikolaev, C. B. Huffman, F. J. Rodriguez-Macias, P. J. Boul, A. H. Lu, D. Heymann, and D. T. Colbert, Appl. Phys. A **67**, 29 (1998).
[17]Z. Chen, I. Santodo, R. Wang, L. F. Xie, H. Y. Mao, H. Huang, Y. Z. Wang, X. Y. Gao, Z. K. Chen, A. T. S. Wee, and W. Chen, Appl. Phys. Lett. **96**, 213104 (2010).

[18]J. Meyer, P. R. Kidambi, B. C. Bayer, C. Weijtens, A. Kahn, A. Centeno, A. Pasquera, Z. Zurutuza, J. Robertson, and S. Hofmann, Sci. Rep. **4**, 5380 (2014).
[19]S. Sanders, A. Cabrero-Vilatela, P. R. Kidambi, J. R. Alexander-Webber, C. Weijtens, P. Braeuninger-Weimer, A. L. Aria, M. Oasim, T. D. Wilkinson, J. Robertson, S. Hofmann, and J. Meyer, Nanoscale **7**, 13135 (2015).
[20]L. D'Arsie, S. Esconjauregui, R. S. Weatherup, X. Wu, W. E. Arter, H. Sugime, C. Cepek, and J. Robertson, RSC Adv. **6**, 113185 (2016).
[21]S. Esconjauregui, L. D'Arsie, Y. Guo, J. W. Yang, H. Sugime, S. Caneva, C. Cepek, and J. Robertson, ACS Nano **9**, 10422 (2015).
[22]S. L. Hellstrom, M. Vogueritchian, R. M. Stoltenberg, I. Irfan, M. Hammock, Y. B. Wang, C. C. Jia, X. Guo, Y. L. Gao, and Z. Bao, Nano Lett. **12**, 3574 (2012).
[23]D. Kondo, H. Nakano, B. Zhou, I. Akiko, K. Hayashi, M. Takahashi, S. Sato, and N. Yokoyama, in *Proceedings of the IEEE International Interconnect Technology Conference (IITC)*, 2014, p. 189.
[24]U. Detlaff-Weglikowski, V. Skakalova, R. Graupner, S. H. Jhang, B. H. Kim, H. J. Lee, L. Ley, J. W. Park, D. Tomanek, and S. Roth, J. Am. Chem. Soc. **127**, 5125 (2005).
[25]M. S. Dresselhaus and G. Dresselhaus, Adv. Phys. **30**, 139 (1981).
[26]W. Zhao, P. H. Tan, J. Liu, and A. C. Ferrari, J. Am. Chem. Soc. **133**, 5941 (2011).
[27]J. Meyer, R. Khalandovsky, P. Görrn, and A. Kahn, Adv. Mater. **23**, 70 (2011).
[28]J. Meyer, S. Hamwi, M. Kroger, W. Kowalsky, T. Reidl, and A. Kahn, Adv. Mater. **24**, 5408 (2012).
[29]S. J. Clark, M. D. Segall, and C. J. Pickard, Z. Kristallogr. **220**, 567 (2005).
[30]S. J. Clark and J. Robertson, Phys. Rev. B **82**, 085208 (2010).
[31]A. Tkatchenko and M. Scheffler, Phys. Rev. Lett. **102**, 073005 (2009).
[32]S. Grimme, J. Comput. Chem. **27**, 1787 (2006).
[33]T. Hu and I. C. Gerber, J. Phys. Chem. C **117**, 2411 (2013).
[34]W. E. Arter, L. D'Arsie, X. Wu, C. S. Esconjauregui, and J. Robertson, Appl. Phys. Lett. **110**, 223104 (2017).
[35]D. Zhan, L. Sun, Z. H. Ni, L. Liu, X. F. Fan, Y. Wang, T. Yu, Y. M. Lam, W. Huang, and Z. X. Shen, Adv. Funct. Mater. **20**, 3504 (2010).
[36]Y. Song, W. Fang, A. L. Hsu, and J. Kong, Nanotechnology **25**, 395701 (2014).
[37]W. Liu, J. Wang, and K. Banerjee, IEEE Electron Device Lett. **37**, 1246 (2016).
[38]K. K. Kim, A. Reina, Y. Shi, H. Park, L. J. Li, Y. H. Lee, and J. Kong, Nanotechnology **21**, 285205 (2010).
[39]K. C. Kwon, K. S. Choi, and S. Y. Kim, Adv. Funct. Mater. **22**, 4724 (2012).
[40]X. Meng, S. Tongay, J. Kang, Z. Chen, F. Wu, S. Li, J. B. Xia, J. Li, and J. Wu, "$FeCl_3$ doping," Carbon **57**, 507 (2013).
[41]Y. Li and Q. Yue, Physica B **425**, 72 (2013).
[42]S. Chuang, C. Battaglia, A. Azcatl, S. McDonnell, K. S. Kang, R. M. Wallace, and A. Javey, Nano Lett. **14**, 1337 (2014).
[43]Y. Guo, D. Liu, and J. Robertson, ACS Appl. Mater. Interfaces **7**, 25709 (2015).
[44]Y. Guo and J. Robertson, Appl. Phys. Lett. **105**, 222110 (2014).
[45]R. A. Nistor, D. M. Newns, and G. J. Martyna, ACS Nano **5**, 3096 (2011).